Proceedings of XIX International Scientific Conference "New Technologies and Achievements in Metallurgy, Material Engineering, Production Engineering and Physics", Częstochowa, Poland, June 7–8, 2018

Effect of Silver Content in $Zr_{55}Cu_{30}Ni_5Al_{10-x}Ag_x$ Alloys on the Supercooled Liquid Stability Analysed by TTT Diagrams

B. Michalski*, P. Blyskun, J. Latuch and W. Kaszuwara
Faculty of Materials Science and Engineering, Warsaw University of Technology,
Wołoska 141, 02-507 Warsaw, Poland

The aim of this work was to investigate influence of silver content on the supercooled liquid stability of $Zr_{55}Cu_{30}Ni_5Al_{10-x}Ag_x$ ($x = 0$–4) alloys which exhibit the compressive strength above 2 GPa. Series of isothermal heating examinations were performed by the differential scanning calorimeter. Based on results, time–temperature–transformation diagrams were created. For the practical testing of time–temperature–transformation curves, thermoplastic deformations in the range of supercooled liquid region were performed. The temperature and time of deformation were controlled according to research results. The time–temperature–transformation diagrams allow for deformation of the samples in a range of stress 40–100 MPa and do not change the structure of the processed samples.

DOI: 10.12693/APhysPolA.135.215
PACS/topics: amorphous materials, phase transformation, phase diagrams, thermal properties, bulk metallic glasses

1. Introduction

Metallic glasses represent a group of modern materials generally made of metals with a metastable amorphous structure. These unique materials exhibit an extraordinary set of properties such as good corrosion and wear resistance, high compression strength, very high toughness or more functionalities such as soft magnetic properties, i.e. Fe-based one [1, 2]. The most popular bulk metallic glasses (BMGs) group is currently the (Zr–Cu)-based one as it combines high mechanical strength with excellent glass forming ability. Due to the glassy structure, these alloys can be successfully transformed at an elevated temperature using hydraulic press, similarly to the polymer materials [3, 4].

Any prolonged annealing above T_g may cause the crystallization to occur, where the amorphous structure begins to vanish. Thermoforming processes used to alter the shape of BMGs exploit this supercooled liquid state and its properties [5–7]. Unfortunately, time, temperature, as well as strain rate increase the risk of crystallization. Using a time–temperature–transformation (TTT) diagram usually supports proper conditions selection for the forming processes of an alloy [8]. In the TTT diagram one can find useful information about potential time and temperature ranges still safe from any possible transformations. The authors of this work successfully created several TTT diagrams of the (Zr–Cu)-based alloys in order to broaden the knowledge of the supercooled liquid stability. The stability was determined by isothermal annealing processes performed at various temperature levels between T_g and T_x. The $Zr_{55}Cu_{30}Ni_5Al_{10}$ alloy was selected as the initial one as it exhibits relatively large ΔT_{xg} and has already been well recognized as a good metallic glass forming alloy [9].

It is known that some minor additions of silver may increase or decrease the glass forming ability of Zr–Cu–Al alloys depending on the relative amount of these elements [10–13].

2. Material and methods

The master $Zr_{55}Cu_{30}Ni_5Al_{10-x}Ag_x$ ($x = 0$–4) alloys were prepared by triple arc melting of pure elements (5N) under argon protective atmosphere with a subsequent removal of an oxides layer. Rod shape samples with diameter of 3 mm were produced by copper mould casting method under argon atmosphere. X-ray diffraction (XRD) method (Rigaku Miniflex2 with Cu K_α radiation) was used to examine the cross-section of these rods to ensure the glassy structure.

Differential scanning calorimetry (DSC, Perkin Elmer DSC-8000) allowed to record thermal effects during heating samples with heating rates of 0.33, 0.67, and 1.22 K/s. The activation energies of crystallization process were calculated by the Kissinger method. Pyris software was used to determine all characteristic temperatures from the obtained DSC curves. The T_g was determined in the inflection point of the curve.

The isothermal annealing was performed at various temperature levels between T_g and T_x, where the time to the crystallization occurrence was measured in order to describe the supercooled liquid thermal stability. Each sample was heated from the room temperature to a particular temperature level with a maximum heating rate (1.67 K/s) and then immediately switched into the isothermal mode. The obtained results were analysed and a time–temperature–transformation (TTT) diagrams were created for all alloys.

*corresponding author; e-mail: b.michalski@inmat.pw.edu.pl

The Vickers microhardness (Hanemann hardness tester) was measured with a load of 50 g. Microhardness was measured on the polished cross-section of the rods. Compression tests were performed on Zwick/Roell testing machine with strain rate of 1×10^{-4} s^{-1}. The gauge dimension of specimens was 3 mm in diameter and 4.5 mm in height. Thermoplastic deformation was performed on specially designed hydraulic press, working in vacuum environment and equipped with induction heating device. Samples were compressed under the lowest possible to achieve strain rate of 3.3×10^{-3} s^{-1}. Dimension of the samples was the same as in compression tests.

3. Results and discussion

The manufactured alloys were examined by XRD method and for all of them typical broad halo was observed. Specimens were also subjected to compressive strength tests (Table I). The $Zr_{55}Cu_{30}Ni_5Al_9Ag_1$ alloy exhibited the highest σ_c value (2.071 GPa). The SEM observations of fractures of the alloys (not included here) showed presence of a characteristic vein-like pattern visible on entire images, which is commonly observed on the fracture surfaces of compressed samples for fully amorphous material.

TABLE I

Characteristic temperatures, microhardness and compression strength of the investigated alloys.

Ag [at.%]	T_g [K]	T_x [K]	ΔT_{gx} [K]	E_a [kJ/mol]	HV0.05	σ_c [GPa]
0	706	781	75	191	768	2.024
1	713	788	75	200	943	2.071
2	708	786	78	198	655	1.983
3	701	781	80	179	866	1.997
4	697	775	78	171	888	1.676

The entire series of the alloys were examined by DSC method for thermal effects. All five DSC curves show the characteristic endothermic peak arising from the glass transition (T_g is defined as the inflexion point). It can be noticed that by addition of silver, characteristic temperatures are shifted to higher values (Table I). However, further increase of Ag content monotonically decreases thermal stability of the alloys. It is clearly visible that T_g, T_x and E_a are in good correlation. The same relationship is observed for mechanical properties. The highest value of compression strength is achieved for the alloy with 1 at.% addition of silver. On the other hand, influence of silver addition on microhardness cannot be clearly determined.

In further DSC examinations, the assumed method for the isothermal annealing was to heat the sample with a maximum heating rate to a given temperature level and hold it there until it crystallizes. A crystallization start time t_x, time to maximal intensity of crystallisation t_p, and time of the end of phase transformation were determined from the isothermal curves. Figure 1 shows obtained times for $Zr_{55}Cu_{30}Ni_5Al_{10}$ alloy. Presented results are in quite good correlation to logarithmic function. Samples were also investigated by XRD to determine change of the amorphous structure after heat treatment. Selected times of isothermal heating at 740 K, marked in Fig. 1, were 60, 120 and 3000 s, respectively. XRD patterns of the samples are presented in Fig. 2. Sample heated for $t_1 = 1$ min shows typical halo for amorphous structure. Heating for two minutes, which is enough to cross T_x line, leads to partial crystallisation of the alloy visible by occurrence of two small peeks of unidentified phases. Further increase of annealing time up to 50 min, causes a crystallisation of primary amorphous phase and enhancement of visible peaks.

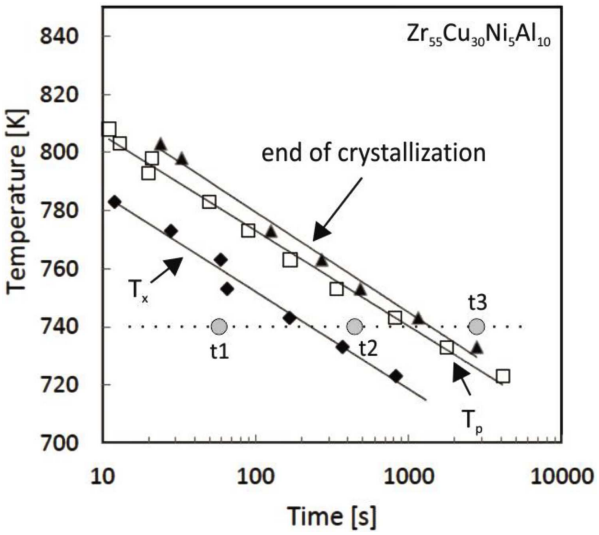

Fig. 1. Correlation between temperature and time collected by the DSC isothermal annealing curves for the $Zr_{55}Cu_{30}Ni_5Al_{10}$ alloy (a half logarithmic scale).

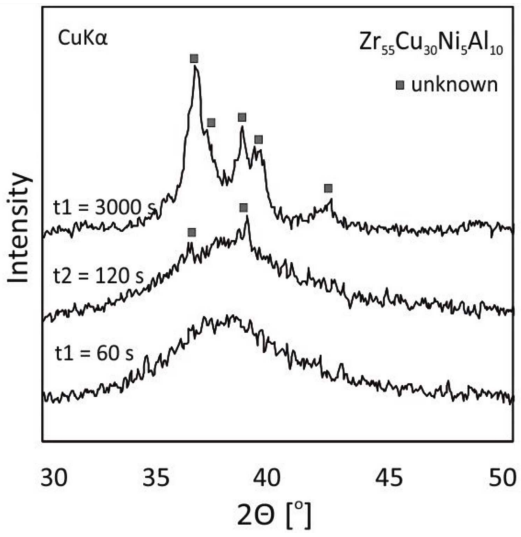

Fig. 2. Time–temperature–transformation diagram for the $Zr_{55}Cu_{30}Ni_5Al_{10}$ alloy.

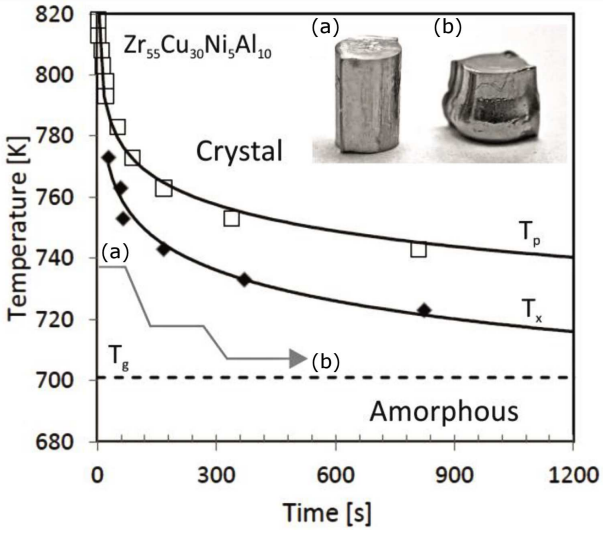

Fig. 3. XRD patterns for the $Zr_{55}Cu_{30}Ni_5Al_{10}$ alloy annealed at 740 K for different times.

In Fig. 3, the same results are presented in linear scale which is typical for the TTT diagrams. The marked T_g line represents value acquired at heating rate 0.666 K/s. By using this plot, one can read necessary information about the supercooled liquid stability of the investigated alloy. For example, heating the alloy, into supercooled liquid region (to the 720 K) and holding this temperature, gives stability of amorphous phase of around $\approx$ 13 min, giving a time to perform thermoplastic deformation process. From practical point of view, more important time is t_x because after reaching this time, heat accumulated in sample is enough to exceed energy required to start the crystallisation of metastable phase. Thus, in further TTT diagrams, this parameter ware plotted as a phase transition line. Additionally, in this figure a scheme of the procedure of practical examination test, which is described in further part of the article, is also visible.

In Fig. 4 TTT diagram presents influence of silver addition on thermal stability. For better clarity, plots were divided onto separate diagrams. Analysing Fig. 4a, it can be noticed that addition of 1 at.% of silver, increase time needed to start crystallisation e.g. for this alloy the amorphous phase is stable at temperature 715 K for $\approx$ 46 min, which is over twice more than for initial alloy ($\approx$ 20 min). On the other hand, further increase of silver content results in a monotonic shift of the phase transition curve to the left side of the diagram and decrease of its thermal stability (Fig. 4b). However, thermal stability is still higher for alloys containing 1–3 at.% of silver than for the initial alloy. In the $Zr_{55}Cu_{30}Ni_5Al_6Ag_4$ alloy, rapid decrease of the thermal stability can be noticed. In the same example at temperature 715 K, time needed for crystallisation is reduced to $\approx$ 12 min.

Minor addition of silver (1 at.%) to the initial $Zr_{55}Cu_{30}Ni_5Al_{10}$ alloy substitutes aluminium atoms and affects mechanical properties (Table I) and thermal stability of the BMGs (Fig. 4). It is caused by the change of free volume (FV) of metallic glass. Values of heat of

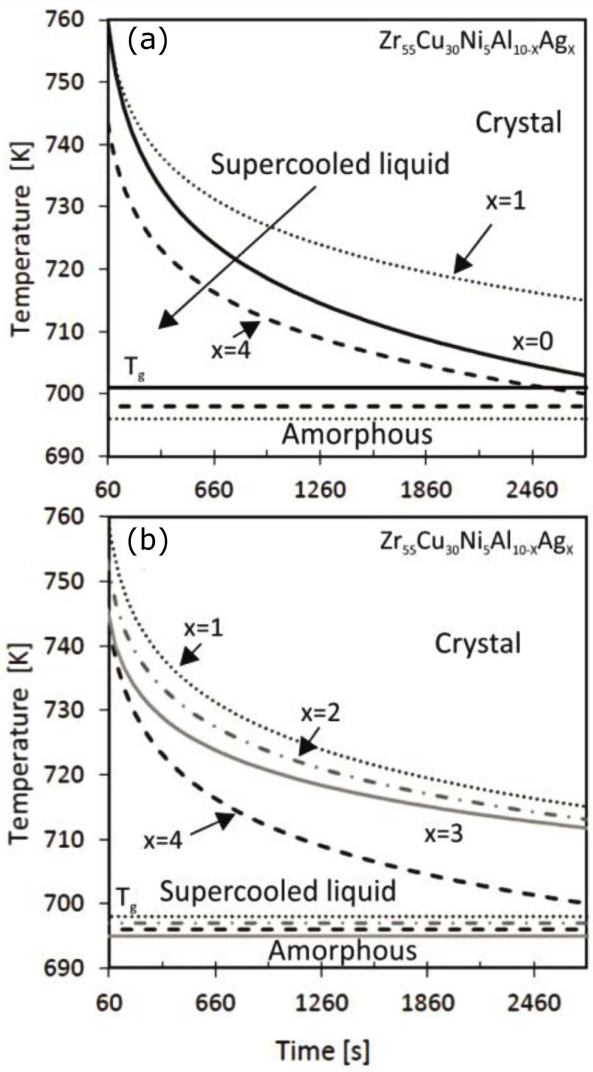

Fig. 4. TTT diagrams of the $Zr_{55}Cu_{30}Ni_5Al_{10-x}Ag_x$ (x = 0–4 at.%) alloys.

mixing for Ag–Al, Ag–Ni, Ag–Cu, Ag–Zr atom pairs are −4, 15, 2, −20 kJ/mol, and for Al–Ni, Al–Cu and Al–Zr pairs are –22, –1, –44 kJ/mol, respectively. This suggests that the only one reasonable mixing is substitution of Al and forming Ag–Zr pairs of atoms [14]. Moreover, atomic radius of silver (144 pm) and aluminium (143 pm) are very close. Silver atoms are slightly larger and can therefore proceed densification of atoms packages and change FV of BMGs. However, further increase of silver content results in increase of FV which leads to decrease of mechanical properties even below these for the initial alloy. On the other hand, thermal stability is still higher, but its decrease is observed. Addition of more than 3 at.% of silver results in drop of thermal stability below the level of the initial alloy.

For practical testing of obtained TTT diagrams, thermoplastic deformation was performed. For each sample procedure was the same and assumed heating to high temperature, when supercooled liquid is still present,

and start deformation until flow stress is reached. Then load was reduced, temperature was changed to lower value and another deformation occurred until flow stress was reached. The mentioned procedure was schematically plotted in Fig. 3. The inset in this figure shows also photographs of the processed samples before and after the treatment. The time of deformation was controlled according to the TTT diagrams. As a result of this experiment, flow stress vs. temperature was plotted (Fig. 5).

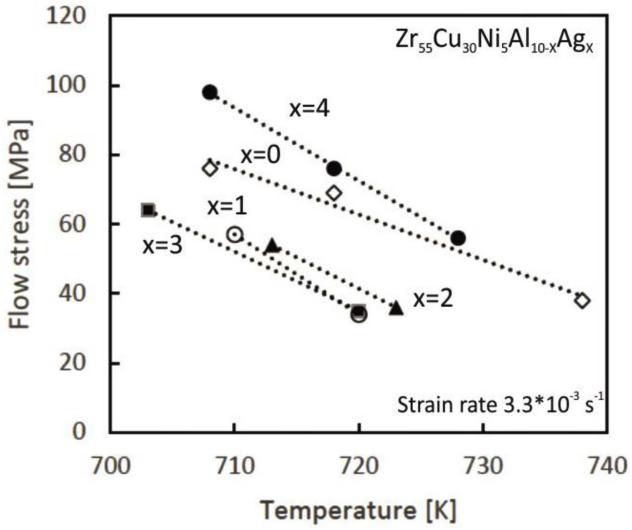

Fig. 5. Dependence of temperature on flow stress of thermoplastic deformation in supercooled liquid region of the $Zr_{55}Cu_{30}Ni_5Al_{10-x}Ag_x$ ($x = 0$–4 at.%) alloys.

It can be noticed that deformation applied at higher temperature of the supercooled liquid region, results in a decrease of flow stress. On the other hand, it decreases also the time of "safe" processing. For the alloys containing 1–3 at.% of silver, flow stress was achieved at lower values than for the initial alloy. However, deformation of the $Zr_{55}Cu_{30}Ni_5Al_6Ag_4$ alloy requires higher stress than the alloy without silver. Samples after thermoplastic deformation were analysed by XRD method. No change of amorphous structure was observed for all samples which confirms usefulness of the obtained TTT diagrams.

4. Conclusions

In this work the influence of silver addition on the glass forming ability and on the mechanical properties in the $Zr_{55}Cu_{30}Ni_5Al_{10-x}Ag_x$ alloys was investigated. Thermal stability of supercooled liquid was determined on a basis of the TTT diagrams. Several conclusions can be established:

- amorphous $Zr_{55}Cu_{30}Ni_5Al_{10-x}Ag_x$ ($x = 1$–4 at.%) alloys can be manufactured successfully by copper mould casting method (rods with diameter of 3 mm),
- thermal stability, represented by the value of T_x, of the amorphous rods was the highest (788 K) for the alloy containing 1 at.% of silver. This alloy has the highest activation energy (200 kJ/mol), the highest mechanical properties (microhardness of 943 HV0.05 and compression strength of 2.071 GPa) and the broadest thermal stability of supercooled liquid amongst investigated alloys basing on the TTT diagrams,
- further silver content increasing (above 3 at.%) results in a drastic drop of thermal stability of the supercooled liquid,
- thermoplastic deformation at temperature of supercooled liquid region (strain rate of 3.3×10^{-3} s^{-1}) leads to Newtonian flow and allows for deformation of the samples by using stress in a range 40–100 MPa without changing the structure of the processed samples.

Acknowledgments

Financial support, provided by the National Science Centre on the basis of a decision No. DEC-2012/05/N/ST8/03728, is gratefully acknowledged.

References

[1] R. Babilas, A. Radon, P. Gebara, *Acta Phys. Pol. A* **131**, 726 (2017).
[2] R. Nowosielski, M. Kądziolka-Gawel, P. Gebara, D. Szyba, R. Babilas, *Acta Phys. Pol. A* **131**, 1212 (2017).
[3] J. Schroers, *Adv. Mater.* **22**, 1566 (2010).
[4] G. Duan, A. Wiest, M.L. Lind, J. Li, W.K. Rhim, W.L. Johnson, *Adv. Mater.* **19**, 4272 (2007).
[5] J. Ragani, A. Volland, S. Calque, Y. Liu, S. Gravier, J.J. Blandin, M. Suery, *J. Alloys Comp.* **504**, S267 (2010).
[6] J. Schroers, T. Nguyen, S. O'Keeffe, A. Desai, *Mater. Sci. Eng. A* **449–451**, 898 (2007).
[7] D. Wang, T. Shi, J. Pan, G. Liao, Z. Tang, L. Liu, *J. Mater. Process. Technol.* **210**, 684 (2010).
[8] D. Wang, G. Liao, J. Pan, Z. Tang, P. Peng, L. Liu, T. Shi, *J. Alloys Comp.* **484**, 118 (2009).
[9] A. Inoue, *Acta Mater.* **48**, 279 (2000).
[10] G.Q. Zhang, Q.K. Jiang, L.Y. Chen, M. Shao, J.F. Liu, J.Z. Jiang, *J. Alloys Comp.* **424**, 176 (2006).
[11] D.V. Louzguine-Luzgin, G. Xie, W. Zhang, A. Inoue, *Mater. Sci. Eng. A* **465**, 146 (2007).
[12] P. Blyskun, G. Cieslak, M. Kowalczyk, J. Latuch, T. Kulik, *Inżynieria Materiałowa* **04**, 154 (2015) (in Polish).
[13] P. Blyskun, J. Latuch, T. Kulik, *Arch. Metall. Mater.* **62**, 1749 (2017).
[14] A. Takeuchi, A. Inoue, *Mater. Trans. JIM* **46**, 2817 (2005).